FDA-MIMO for target localization via multi-pulse tensor decomposition

Yibin Liu[1] , Chunyang Wang[1], Jian Gong[1] and Ming Tan[2]

[1]Air and missile Defense College, Air Force Engineering University, Xi'an, China and [2]College of Information and Communication, National University of Defense Technology, Changsha, China

Abstract

By combining multiple input multiple output (MIMO) technology and multiple matched filters with frequency diverse array (FDA), FDA-MIMO radar can be used to achieve two-dimensional target localization with range and angle. In this paper, we propose two FDA-MIMO multi-pulse target localization methods based on tensor decomposition. Based on the canonical polyadic decomposition theory, the signal models of CPD-DP-FDA with double-pulse and CPD-SP-FDA with stepped frequency pulses are established. By analyzing the signal processing procedures of the two schemes, the indicator beampattern used for target localization is obtained. The parameter estimation accuracy of the proposed method is investigated in single target and multiple targets scenarios, and the proposed method is compared with the traditional double-pulse method. The results show that the target localization method based on tensor decomposition can effectively solve the problem of multi-target indication ambiguity. The target positioning effect can be further improved by combining stepped frequency pulses. The derivation of Cramer–Rao Lower Bound (CRLB) demonstrates the superiority of the method.

Introduction

Unlike traditional phased array radar, multiple input multiple output (MIMO) radar not only improves the reliability of target detection and the ability to detect stealth targets, but also has the advantages of high resolution, high target parameter estimation accuracy, anti-interference, and better target recognition capabilities. Antonik first proposed the concept of frequency diverse array (FDA) radar at the IEEE International Radar Conference [1]. The beampattern of FDA radar is range-angle-dependent, which provides the possibility for joint positioning of the target's range and angle parameters. Integrating the system characteristics of frequency diverse array and MIMO radar, frequency diversity array MIMO (FDA-MIMO) radar [2–5], a new type of radar system, has attracted widespread attention.

FDA-MIMO radar can form an equivalent transmit beampattern, so that the transmission information can be integrated into the receiving end. It achieves a more flexible use of the range-dimensional freedom and improves the capability of range-angle two-dimensional joint signal processing. Making full use of the characteristics of FDA-MIMO can achieve range-angle two-dimensional target localization [6] and anti-mainlobe false target interference [7]. The influence of frequency offset error on the beamforming and target positioning performance of FDA-MIMO radar is analyzed in [8]. In [9], the Cramer–Rao Lower Bound (CRLB) of the FDA-MIMO radar was derived, and the transmitter was designed to minimize the CRLB of the system on this basis. The target detection performance of the FDA-MIMO system radar was analyzed in [10]. The performance of moving target parameter estimation of frequency diverse array radar was analyzed in [11] and compared with the performance of phased array radar. In [12], a double-pulse parameter estimation method based on frequency diverse array radar was proposed. In [13], the double-pulse method was extended to the FDA-MIMO radar system, which further improved the target range-angle localization performance. A precise response control algorithm was proposed in [14] to achieve precise control of the range-angle beampattern to enhance the robustness of the FDA-MIMO radar system. Based on the generalized likelihood ratio test criterion, the method of designing an FDA-MIMO adaptive detector was studied in [15]. In [16], a range-dimensional interference suppression adaptive beamforming method based on the FDA-MIMO radar system was proposed to further improve the target positioning performance. In [17], the method of using FDA-MIMO range-dependent adaptive beamforming to achieve range-dependent interference suppression in target positioning was analyzed. The FDA-MIMO anti-jamming algorithm based on eigenvalue projection and block matrix processing was proposed in [18]. Based on the coherent frequency diversity array system, [19] designed a space-time filter for interference suppression. In [20], the simulated annealing algorithm of the FDA-MIMO system was proposed to combat the deception interference of the mainlobe range dimension. Combining polarization characteristics, frequency diverse array and MIMO system, [21] explored ways

to increase the output signal-to-interference and noise ratio to enhance the radar's anti-jamming performance. The time-invariant problem of the beampattern during target indication is also of interest. In [22], a leading group proposed two types of time-modulated frequency diverse arrays to achieve time-invariant focusing of multiple targets in space. Similarly, the concentration of energy at single or multiple target locations was achieved in [23] by optimizing the time-modulated frequency offset. However, the above method is designed with the idea of obtaining a stable gain at the target position only, with the gain remaining time-varying at other positions. Thus, [24] conducted a reasonable analysis of the time parameters in the FDA system based on the principle of wave propagation, which provide guidance for the expansion of FDA-MIMO applications under consideration of time parameters.

As a form of data representation, tensor is provided with rich theoretical connotation by multilinear algebra theory. One of the most important applications is the development of effective tensor decomposition methods under the framework of multilinear theory. In the past 10 years or so, two typical decompositions of tensors, CPD and HOSVD, have been extensively studied in array signal processing [25, 26]. As early as 2000, a DOA estimation algorithm based on a uniform linear array in [27] was first proposed in combination with CPD. In [28], CPD was extended to DOA estimation based on MIMO radar, and the identification and estimation performance of the algorithm were discussed under different transmission modes and different signal models. Tensor decomposition was applied to MIMO radar angle estimation in [29], which realizes an algorithm that does not require spectral peak search and angles are automatically paired. In [30], the DOA was solved by modeling the MIMO radar covariance tensor. Recently, the trilinear model in tensor theory has been introduced in [31] for monostatic FDA-MIMO radar to achieve range and angle parameter estimation. This is a good example of the promising application of tensor theory in FDA radar.

In this paper, a double-pulse target localization scheme based on canonical polyadic decomposition (CPD-DP-FDA) is proposed by introducing tensor decomposition into FDA-MIMO. After receiving the data containing the target information, the tensor signal model is used to replace the traditional signal model for processing. By using the correspondence of the factor matrix in tensor decomposition, the problem of ambiguity in multi-target localization in traditional double-pulse FDA is effectively solved [12]. Finally, a stepped frequency pulse target localization scheme based on tensor decomposition (CPD-SP-FDA) is proposed. Finally, the effects of the two CPD-based schemes and the traditional double-pulse scheme are compared, and the numerical simulation demonstrates the superiority of the proposed scheme.

Notation: Boldfaced lowercase letters, such as $\boldsymbol{l}$, represent vectors, and boldfaced uppercase letters, such as $\boldsymbol{L}$, denote matrixes. The letter variants, such as ℓ, represent tensors. ° denotes the outer product operation on the vector, while $\odot$ denotes the Hadamard product. The transpose, conjugate, and conjugate transpose of a matrix or a vector are denoted by $(\cdot)^T$, $(\cdot)^*$, and $(\cdot)^H$, respectively, while $\otimes$ denotes the Kronecker product.

Mechanism of tensor decomposition

The target information is implicit in the received sample, and the received sample or sample covariance needs to be decomposed. Tensor decomposition is a means to achieve low-rank approximation of tensors. Compared with matrix factorization, the difference is:

because tensor factorization mines the structure information of the data more, it has better identification or achieves more accurate decomposition. These advantages make it be introduced into the field of array signal processing to improve the performance of DOA estimation. The canonical polyadic decomposition (CPD) used in this paper is introduced below.

Consider a tensor ℓ with rank K and dimension R.

$$\ell = \sum_{k=1}^{K} \mathbf{l}_1^k \circ \mathbf{l}_2^k \circ \ldots \circ \mathbf{l}_R^k, \tag{1}$$

where $\mathbf{l}_r^k$ is the kth component $k = 1, 2, \ldots, K$ corresponding to the rth dimension.

The purpose of CPD is to represent a tensor as a sum of rank 1 tensors. The number of rank 1 tensors is the rank of the entire tensor. The schematic diagram of CPD based on the third-order tensor is shown in Fig. 1.

CPD directly decomposes the tensor into the sum of each rank 1 tensor, and uses the structural information of the tensor to decompose it into the various factors themselves. Taking a third-order tensor as an example, if it can be expressed by (1), then the r-module matrix expansion along the three dimensions can be expressed as

$$\ell_{(1)} = \mathbf{L}_1(\mathbf{L}_2 \odot \mathbf{L}_3)^T \tag{2a}$$

$$\ell_{(2)} = \mathbf{L}_2(\mathbf{L}_3 \odot \mathbf{L}_1)^T \tag{2b}$$

$$\ell_{(3)} = \mathbf{L}_3(\mathbf{L}_2 \odot \mathbf{L}_1)^T \tag{2c}$$

where $\mathbf{L}_1 = [\mathbf{l}_1^1, \mathbf{l}_1^2, \ldots, \mathbf{l}_1^K]$, $\mathbf{L}_2 = [\mathbf{l}_2^1, \mathbf{l}_2^2, \ldots, \mathbf{l}_2^K]$, $\mathbf{L}_3 = [\mathbf{l}_3^1, \mathbf{l}_3^2, \ldots, \mathbf{l}_3^K]$ are the matrix factors that constitute the tensor. Equation (2) shows the relationship between the tensor and the matrix factors obtained after the modulus r is expanded. For the received sample of the multi-dimensional array, assuming that the array size is $I_1 \times I_2 \times \cdots \times I_R$, the sample received by an element in the array at time t can be expressed as [32]

$$x_{i_1,\ldots,i_R}(t) = \sum_{k=1}^{K} l_{i1} \ldots l_{iR}(\mu_k)s_k(t) + n_{i1,\ldots,iR}, \tag{3}$$

where l_{ir} denotes the i_rth element in the rth dimension in the array, $\mathbf{s}_k(t)$ denotes the sampling at the time t of the kth signal, $n(t)$ denotes the noise item received at the time t, and μ_k denotes the parameter vector of the kth signal. The specific form is decided. The steering vector of the kth signal corresponding to the rth dimension of the array is $\boldsymbol{l}_r(\mu_{r,k})$. Then the sample vector $\boldsymbol{x}(t) \in \mathbb{C}^{\prod_{i=1}^{R} I_i \times 1}$ received by the entire array at time t can be expressed as

$$\boldsymbol{x(t)} = \sum_{k=1}^{K} \mathbf{l}(\mu_k)\mathbf{s}_k(t) + \mathbf{n}(t). \tag{4}$$

The steering vector of the entire array can be expressed by the Khatri–Rao product of the steering vectors of each dimension as

$$\mathbf{l}(\mu_k) = \overset{R}{\underset{r=1}{\odot}} \mathbf{l}_r(\mu_{r,k}), \tag{5}$$
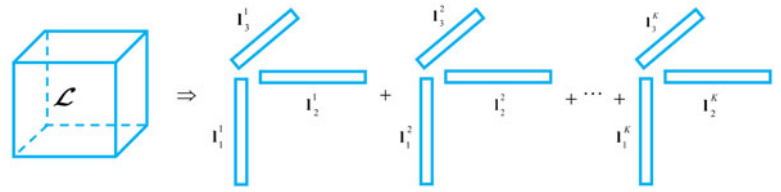
Fig. 1. Schematic diagram of the third-order tensor CPD.

where $\mathbf{l}_r$ is the steering vector $\mathbf{l}_r \in \mathbb{C}^{I_r \times 1}$ corresponding to the kth signal in the rth dimension of the multi-dimensional array, I_r is the size of the rth dimensional array, and $\mu_{r,k}$ denotes the parameter of the kth signal in the rth dimension of the multi-dimensional array.

The received data of the entire array can be expressed as a tensor form $\mathcal{X}(t) \in \mathbb{C}^{I_1 \times I_2 \times \cdots \times I_R}$. For a total of T time samples, the tensor mode of the array received data can be expressed by the cascade of sub-tensors at each time as

$$\mathcal{X} = \mathcal{X}(1) \cup_{R+1} \mathcal{X}(2) \cup_{R+1} \ldots \cup_{R+1} \mathcal{X}(T), \qquad (6)$$

where $\cup_{R+1}$ denotes that two tensors are concatenated along the rth dimension. Thus, the received data can be constructed as

$$\mathcal{X} = \mathcal{L} \times_{R+1} \mathbf{S} + \mathcal{N} \qquad (7)$$

where $\mathcal{X}$ is the sample tensor form $\mathcal{X} \in \mathbb{C}^{I_1 \times I_2 \times \cdots \times I_R \times T}$ of the multi-dimensional array, $\mathcal{L}$ is the steering tensor of the multi-dimensional array, whose dimension is $\mathcal{L} \in \mathbb{C}^{I_1 \times I_2 \times \cdots \times I_R \times K}$, $\mathbf{S}$ denotes the signal matrix, and $\mathcal{N}$ denotes the noise contained in the T samples received by the multi-dimensional array. Then the steering tensor of the kth signal can be expressed by the outer product of the steering vectors of each dimension as

$$\mathcal{L}_k(\mu_k) = \mathbf{l}_1(\mu_{1,k}) \circ \mathbf{l}_2(\mu_{2,k}) \circ \ldots \circ \mathbf{l}_R(\mu_{R,k}). \qquad (8)$$

Thus, the estimation of the array steering vector can be obtained by CPD.

Signal model of FDA-MIMO radar

Consider an FDA-MIMO scheme in which both transmit and receive arrays are uniform linear arrays, as shown in Fig. 2. The transmitted carrier frequency is f_0, and the transmitted frequency of the nth array element can be expressed as

$$f_n = f_0 + n\Delta f. \qquad (9)$$

The transmitted signal of the nth element can be expressed as

$$s_n(t) = rect\left(\frac{t}{T_p}\right)\psi_n(t)e^{j2\pi(f_0+n\Delta f)t}, \qquad (10)$$

where T_p is the pulse width, $\psi_n(t)$ is the baseband envelope of the nth transmitting array element signal, which satisfies the orthogonality condition as

$$\int \psi_{n1}^*(t) \cdot \psi_{n2}(t - \tau) \, dt = 0, \quad n1 \neq n2, \ \forall \tau. \qquad (11)$$
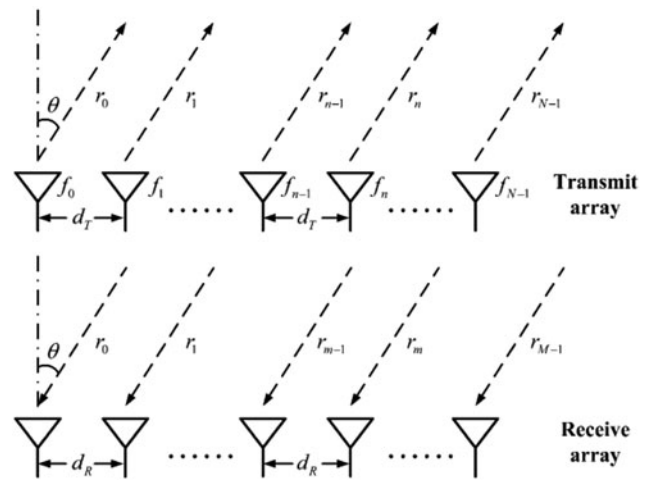

Fig. 2. Schematic diagram of FDA-MIMO radar.

Assuming that there are K targets in the far field, the signal returned from the position (r, θ) and received by the mth received element can be expressed as

$$s_{n,m}(t) = rect\left(\frac{t - \tau_{n,m}}{T_p}\right)\psi_n(t - \tau_{n,m})e^{j2\pi(f_0+n\Delta f)(t-\tau_{n,m})}, \qquad (12)$$

where $\tau_{n,m}$ is the propagation delay from the nth transmitted element to the mth received element, which can be expressed as

$$\tau_{n,m} = 2r_k/c - nd_T\sin\theta_k/c - md_R\sin\theta_k/c \ (1 \leq k \leq K). \qquad (13)$$

Thus, after signal processing at the receiving end, the output signal is obtained as

$$x_{n,m}(t) \approx rect\left(\frac{t - \tau_{n,m}}{T_p}\right)$$
$$\xi_s e^{j2\pi(-f_0(2r_k/c)-n\Delta f(2r_k/c)+f_0((nd_T\sin\theta_k)/c)+f_0((md_R\sin\theta_k)/c))}, \qquad (14)$$

where ξ_s is the signal complex coefficient after matched filtering. When only considering the equivalent transmit beampattern, the above formula can be simplified as

$$x_{n,m}(t) \approx rect\left(\frac{t - \tau_{n,m}}{T_p}\right)\xi_s e^{j2\pi(-f_0(2r_k/c)-n\Delta f(2r_k/c)+f_0((nd_T\sin\theta_k)/c))}. \qquad (15)$$

Then the transmit steering vector can be expressed as

$$\mathbf{S}_t(r_k, \theta_k) = \mathbf{a}(r_k, \theta_k)$$
$$= [1, e^{j2\pi[-\Delta f 2r_k/c + f_0 d_T \sin \theta_k/c]}, \ldots, \qquad (16)$$
$$e^{j2\pi[-(N-1)\Delta f 2r_k/c + (N-1)f_0 d_T \sin \theta_k/c]}]^{\mathrm{T}}.$$

When the frequency increment $\Delta f = 0$ is considered, the transmit steering vector is simplified to

$$\mathbf{S}_{t0}(\theta_k) = [1, e^{j2\pi f_0 d_T \sin \theta_k/c}, \ldots, e^{j2\pi(N-1)f_0 d_T \sin \theta_k/c}]^{\mathrm{T}}. \qquad (17)$$

Double-pulse scheme for the localization of targets

A method for target localization using a double pulse frequency diverse array is proposed in [12]. In this method, two steps are required to separately estimate the angle and range parameters of the target.

The first step is to use the FDA pulse with $\Delta f = 0$ to estimate the target angle parameter. In this case, the data model of the received signal can be written as

$$\boldsymbol{x} = \alpha_0 \mathbf{S}_{t0}(\theta_k) + \mathbf{n}, \qquad (18)$$

where α_0 represents the complex amplitude of the signal, and $\boldsymbol{n}$ is the additive white noise vector. The weight vector using non-adaptive beamforming is expressed as

$$\mathbf{w} = \mathbf{S}_{t0}(\theta_k). \qquad (19)$$

Thus, the formula used to estimate the angle parameter of the target is

$$\hat{\theta}_k = \arg\left\{\max_\theta |\mathbf{w}^{\mathrm{H}} \cdot \mathbf{S}(\theta)|^2\right\}. \qquad (20)$$

The second step is to estimate the range parameter based on the angle parameter information of the first step. The data model of the received signal can be written as

$$\mathbf{x} = \alpha_0 \mathbf{S}_t(r_k, \hat{\theta}_k) + \mathbf{n}. \qquad (21)$$

The weight vector of beamforming can be expressed as

$$\mathbf{w} = \mathbf{S}_t(r_k, \hat{\theta}_k). \qquad (22)$$

Therefore, the formula that can be used to solve the target parameter is

$$\hat{r}_k = \arg\left\{\max_r |\mathbf{w}^{\mathrm{H}} \cdot \mathbf{x}|^2\right\}. \qquad (23)$$

Double-pulse localization scheme based on CPD

The data model of the double pulses signal of the lth snapshot can be written as

$$\boldsymbol{x}(l) = \begin{bmatrix} \mathbf{S}_{t0}(\theta_1) \otimes \mathbf{S}_t(r_1, \theta_1), \mathbf{S}_{t0}(\theta_2) \otimes \mathbf{S}_t(r_2, \theta_2), \\ \ldots, \mathbf{S}_{t0}(\theta_K) \otimes \mathbf{S}_t(r_K, \theta_K) \end{bmatrix} \boldsymbol{s}(l) + \boldsymbol{n}(l), \qquad (24)$$

where $\boldsymbol{s}(l) = [s_1(l), s_2(l), \ldots, s_K(l)]^T$ is composed of the amplitude and phase generated by the K targets in the lth pulse. The noise vector $\mathbf{n}(l)$ obeys the Gaussian distribution whose mean value is zero and the variance is $\sigma^2 \boldsymbol{I}_{NN}$. The entire array flow matrix can be further expressed as

$$\mathbf{S} = [\mathbf{S}_{t0}(\theta_1) \otimes \mathbf{S}_t(r_1, \theta_1), \ldots, \mathbf{S}_{t0}(\theta_K) \otimes \mathbf{S}_t(r_K, \theta_K)]. \qquad (25)$$

Considering that the total sampling times is L, the data matrix form outputted by matched filtering can be expressed as

$$X = (\mathbf{S}_{t0} \odot \mathbf{S}_t)\boldsymbol{S}^T + \boldsymbol{N}, \qquad (26)$$

where $X = [x(1), x(2), \ldots, x(L)] \in \mathbb{C}^{NN \times L}$, $S = [s(1), s(2), \ldots, s(L)] \in \mathbb{C}^{L \times K}$ and noise matrix $N \in \mathbb{C}^{NN \times L}$.

Since (26) satisfies the modulo n expansion form of the tensor third-order PARAFAC model, canonical polyadic decomposition (CPD) can be introduced to achieve target localization. The third-order tensor constructed by the array received data represented by (26) can be expressed as

$$\gamma(g, h, l) = \sum_{k=1}^{K} S_{t0}(g, k)S_t(h, k)S(l, k) + \eta(g, h, l), \qquad (27)$$

where $g = 1, 2, \ldots, G$, $h = 1, 2, \ldots, H$, $l = 1, 2, \ldots, L$. $S_{t0}(g, k)$ represents the element at position (g, k) of the factor matrix $\boldsymbol{S}_{t0}$, $S_t(h, k)$ represents the element at position (h, k) of the factor matrix $\boldsymbol{S}_t$, and $S(l, k)$ represents the element at position (l, k) of the factor matrix $\boldsymbol{S}$. η is the third-order tensor representation of additive white noise.

In the first step, since there is a coupling of range and angle in the FDA's equivalent transmit steering vector, it is necessary to estimate the target angle parameter first. The CPD directly decomposes the tensor into the sum of each rank-1 tensor, which can use the structural information of the tensor to decompose it into the various factors. Considering that the kth column vector of the factor matrix $\boldsymbol{S}_{t0}$ is $\boldsymbol{s}_{tk}$, the phase obtained after normalization to eliminate scale scaling can be expressed as

$$\mu_{tk} = angle(\boldsymbol{s}_{tk}) = [0, \pi \sin \theta_k, \ldots, (G-1)\pi \sin \theta_k]^T. \qquad (28)$$

The weight vector of beamforming can be expressed as

$$\mathbf{w}_{t0} = \exp(j\mu_{tk}) \qquad (29)$$

Thus, the formula that can be used to estimate the angle parameter of the target can be written as

$$\hat{\theta}_k = \arg\left\{\max_\theta |\mathbf{w}_{t0}^{\mathrm{H}} \cdot \mathbf{S}(\theta)|^2\right\}. \qquad (30)$$

The second step is to combine the factor matrix $\boldsymbol{S}_t$ and μ_{tk} in the first step to estimate the range parameter. The kth column vector of the factor matrix $\boldsymbol{S}_t$ is ξ_{tk}. The phase obtained after normalization to eliminate scale scaling can be expressed as

$$\nu_{tk} = angle(\xi_{tk})$$
$$= [0, -4\Delta f \pi r_k/c + \pi \sin \theta_k, \ldots, -4(H-1)\Delta f \pi r_k/c$$
$$+ (G-1)\pi \sin \theta_k]^T, \qquad (31a)$$

$$\varepsilon_{tk} = \nu_{tk} - \mu_{tk}$$
$$= [0, -4\Delta f \pi r_k/c, \ldots, -4(H-1)\Delta f \pi r_k/c]^T. \quad (31b)$$

Thus, the weight vector of beamforming can be obtained as

$$\mathbf{w}_t = \exp\{j\varepsilon_{tk}(r_k)\}. \quad (32)$$

The formula for solving the target parameter can be written as

$$\hat{r}_k = \arg\left\{\max_r |\mathbf{w}_t^{\mathrm{H}} \cdot \mathbf{S}(r, \theta)|^2\right\}. \quad (33)$$

Stepped frequency pulses localization scheme based on CPD

The time frequency schematic diagram of the stepped frequency pulses localization scheme is shown in Fig. 3. The total number of pulses is P. The frequency of the pth pulse of the nth element can be expressed as

$$f_{n,k} = f_0 + n\Delta f + p\Delta f_t, \quad p = 0, 1, \ldots, P-1, \quad (34)$$

where Δf_t is the unit increment of frequency between pulses.

Thus, the transmitted signal of the nth element can be expressed as

$$s_n(t) = \sum_{p=0}^{P-1} rect\left(\frac{t - pT_p}{T_p}\right)\psi_n(t - pT_p)e^{j2\pi(f_0 + n\Delta f + p\Delta f_t)(t - pT_p)}. \quad (35)$$

When observing a target point at (r, θ), the received signal related to the nth transmit array element and the mth receive array element can be expressed as

$$s_{n,m}(t) = \sum_{p=0}^{P-1} rect\left(\frac{t - pT_p - \tau_{n,m}}{T_p}\right)$$
$$\psi_n(t - pT_p - \tau_{n,m})e^{j2\pi(f_0 + n\Delta f + p\Delta f_t)(t - pT_p - \tau_{n,m})}. \quad (36)$$

Thus, after signal processing and matched filtering at the receiver, the approximate signal can be expressed as

$$x_{n,m}(t) =$$
$$\sum_{p=0}^{P-1} \xi_s e^{j2\pi(-f_0(2r/c) - n\Delta f(2r/c) - p\Delta f_t(2r/c) + f_0((nd_T \sin\theta)/c) + f_0((md_R \sin\theta)/c))}. \quad (37)$$

The array factor can be expressed as

$$AF = \sum_{m=0}^{M-1}\sum_{n=0}^{N-1} x_{n,m}(t)$$
$$= \xi_s e^{-j2\pi f_0(2r/c)} \sum_{m=0}^{M-1}\sum_{n=0}^{N-1}\sum_{p=0}^{P-1} \quad (38)$$
$$\xi_s e^{j2\pi(-n\Delta f(2r/c) - p\Delta f_t(2r/c) + f_0((nd_T \sin\theta)/c) + f_0((md_R \sin\theta)/c))}.$$

Thus, the steering vector of the entire array can be written as

$$\mathbf{S} = \mathbf{a}(r, \theta) \otimes \mathbf{p}(r) \otimes \mathbf{b}(\theta), \quad (39)$$

where $\mathbf{a}(r, \theta)$, $\mathbf{p}(r)$, and $\mathbf{b}(\theta)$ can be denoted as

$$\mathbf{a}(r, \theta) = [1, \quad e^{j2\pi[-\Delta f 2r/c + f_0 d_T \sin\theta/c]}, \ldots,$$
$$e^{j2\pi[-(N-1)\Delta f 2r/c + (N-1)f_0 d_T \sin\theta/c]}]^{\mathrm{T}}, \quad (40a)$$

$$\mathbf{p}(r) = [1, \quad e^{-j2\pi\Delta f_t(2r/c)}, \ldots, e^{-j2\pi(P-1)\Delta f_t(2r/c)}]^{\mathrm{T}}, \quad (40b)$$

$$\mathbf{b}(\theta) = [1, \quad e^{j2\pi f_0((d_R \sin\theta)/c)}, \ldots, e^{j2\pi(M-1)f_0((d_R \sin\theta)/c)}]^{\mathrm{T}}. \quad (40c)$$

The transmit steering vector can be expressed as

$$\mathbf{S}_t = \mathbf{a}(r, \theta) \otimes \mathbf{p}(r). \quad (41)$$

To ensure the fairness of the comparison, according to the analysis in [12], the equivalent transmit beampattern is still analyzed here. The data model of the received signal can be expressed as

$$\mathbf{x}_{r,\theta} = \alpha_0 \mathbf{S}_t(r, \theta) + \mathbf{n}. \quad (42)$$

After matched filtering, the data model of the lth snapshot equivalent transmitter signal can be rewritten as

$$x(l) = [\mathbf{S}_t(r_1, \theta_1), \mathbf{S}_t(r_2, \theta_2), \ldots, \mathbf{S}_t(r_K, \theta_K)]s(l) + n(l)$$
$$= \begin{bmatrix} \mathbf{a}(r_1, \theta_1) \otimes \mathbf{p}(r_1), \mathbf{a}(r_2, \theta_2) \otimes \mathbf{p}(r_2), \\ \ldots, \mathbf{a}(r_K, \theta_K) \otimes \mathbf{p}(r_K) \end{bmatrix} s(l) + n(l), \quad (43)$$

where $s(l) = [s_1(l), s_2(l), \ldots, s_K(l)]^T$ is composed of the amplitude and phase generated by the K targets in the lth pulse. The noise vector $n(l)$ obeys the Gaussian distribution whose mean value is zero and the variance is $\sigma^2 \mathbf{I}_{NN}$. Thus the array flow matrix can be further expressed as

$$\mathbf{S} = [\mathbf{a}(r_1, \theta_1) \otimes \mathbf{p}(r_1), \ldots, \mathbf{a}(r_K, \theta_K) \otimes \mathbf{p}(r_K)]. \quad (44)$$

To introduce tensor operations, the above formula can be rewritten in the form of the Khatri–Rao product as

$$\mathbf{S} = \mathbf{a} \odot \mathbf{p}. \quad (45)$$

Considering that the total number of samples is L, the data matrix form outputted by matched filtering can be expressed as

$$X = (\mathbf{a} \odot \mathbf{p})S^T + N, \quad (46)$$

where $X = [x(1), x(2), \ldots, x(L)] \in \mathbb{C}^{NN \times L}$, $S = [s(1), s(2), \ldots, s(L)] \in \mathbb{C}^{L \times K}$ and noise matrix $N \in \mathbb{C}^{NN \times L}$.

Using CPD to obtain localization of the targets, the third-order tensor generated from the data received by the array of (46) can be
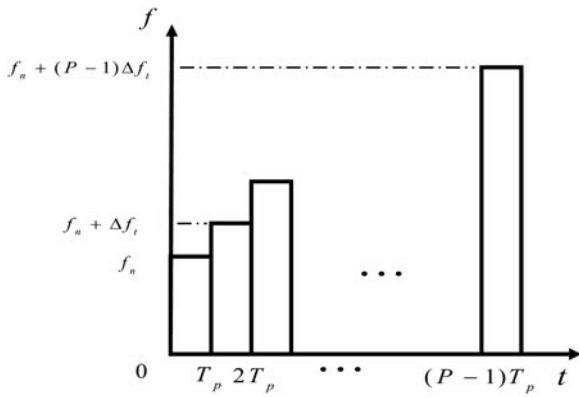
Fig. 3. Schematic diagram of stepped frequency pulse.

constructed as

$$\varpi(i, j, l) = \sum_{k=1}^{K} a(i, k)p(j, k)S(l, k) + \eta(i, j, l), \qquad (47)$$

where $i = 1, 2,\ldots, I, j = 1, 2, \ldots, J, l = 1, 2, \ldots, L$. $a(i, k)$ represents the element at position (i, k) of the factor matrix $\mathbf{a}$, $p(j, k)$ represents the element at position (j, k) of the factor matrix $\mathbf{p}$, and $S(l, k)$ represents the element at position (l, k) of the factor matrix $\mathbf{S}$. η is the third-order tensor representation of additive white noise.

In the first step, due to the coupling of range and angle equivalent transmit steering vector in FDA, it is necessary to estimate the target range parameter first. Considering that the kth column vector of the factor matrix $\mathbf{p}$ is ϕ_k, the phase obtained after normalization to eliminate scale scaling can be expressed as

$$\varphi_k = angle(\phi_k)$$
$$= [0, -4\pi\Delta f_t r/c, \ldots, -4\pi(J-1)\Delta f_t r/c]^T. \qquad (48)$$

The weight vector of beamforming can be expressed as

$$\mathbf{w} = \exp(j\varphi_k). \qquad (49)$$

Then the formula that can be used to estimate the range parameter of the target can be written as

$$\hat{r}_k = \arg\left\{\max_r |\mathbf{w}^H \cdot \mathbf{x}|^2\right\}. \qquad (50)$$

The second step is to estimate the angle parameter based on the factor matrix a and φ_k in the first step. The kth column vector of the factor matrix a is φ_k. Thus, the phase obtained after normalization to eliminate scale scaling can be expressed as

$$\zeta_k = angle(\varphi_k)$$
$$= [0, -4\Delta f \pi r_k/c + \pi \sin\theta_k, \ldots, \qquad (51a)$$
$$-4(J-1)\Delta f \pi r_k/c + (I-1)\pi \sin\theta_k]^T,$$

$$\delta_k = \zeta_k - \varphi_k = [0, \pi\sin\theta_k, \ldots, (I-1)\pi\sin\theta_k]^T. \qquad (51b)$$

The weight vector of beamforming can be obtained as

$$\mathbf{w} = \exp\{j\delta_k(\theta_k)\}. \qquad (52)$$

The formula for solving the target parameter can be written as

$$\hat{\theta}_k = \arg\left\{\max_\theta |\mathbf{w}^H \cdot \mathbf{x}|^2\right\}. \qquad (53)$$

CPD-based localization methods have an additional step of tensor decomposition compared to the traditional method. Its complexity is mainly reflected in iteratively solving the three factor matrices in equations (27) and (47). Assuming that the number of signals is K, the total number of iterations is Q and the number of stepped frequency pulses is L. Then the total computational complexity of the three factor matrices after one iteration in two CPD-based methods are $O(3K^3 + 3KN^2Q + K(N^2 + 2NQ) + 2K^2(N^2 + 2NQ))$ and $O(3K^3 + 3KNLQ + K(NL + NQ + LQ) + 2K^2(NL + NQ + LQ))$, respectively. Finally, all three of the methods require a one-dimensional search. Assuming that the step size of the search is γ, the computational complexity of the search step is $O(\gamma[N^2(N^2 - K) + N^2 - K])$. It indicates that the effect of the variation in the number of array elements on the computational complexity of the CPD algorithm is extremely obvious, and the performance advantage of the method is derived from the higher computational complexity. Thus, it is important to explore the low computational complexity of the decomposition algorithm for the real-time implementation of the method in this paper.

CRLB

Equation (42) can be rewritten as

$$\mathbf{x_u} = \sqrt{\text{SNR}} \cdot \mathbf{u}(r, \theta) + \mathbf{n}, \qquad (54)$$

where SNR is the signal-to-noise power ratio. The mean and variance of the noise vector $\mathbf{n}$ denote all-zero vector and the identity matrix, respectively. When the double pulses FDA scheme in [12] is adopted, $\mathbf{u}(r, \theta)$ can be expressed as

$$\mathbf{u}_D(r, \theta) = [\mathbf{u}(r, \theta)|_{\omega_i}, \mathbf{u}(r, \theta)|_{\omega_0}]^T. \qquad (55)$$

When the stepped frequency pulses FDA scheme is adopted, $\mathbf{u}(r, \theta)$ can be denoted as

$$\mathbf{u}_S(r, \theta) = [\mathbf{a}(r, \theta)|_{\omega_0}, \ldots, \mathbf{a}(r, \theta)|_{\omega_{P-1}}]^T, \qquad (56)$$

where

$$\mathbf{u}(r, \theta)|_{\omega_i} = [1, e^{-j2\pi f_0 \Delta d \sin\theta/c}, \ldots, e^{-j2\pi(N-1)f_0\Delta d \sin\theta/c}], \qquad (57a)$$

$$\mathbf{u}(r, \theta)|_{\omega_0} = \begin{bmatrix} 1, e^{-j[2\pi(f_0+\Delta f)\Delta d \sin\theta/c - 2\pi\Delta fr/c]}, \\ \ldots, e^{-j[(N-1)2\pi(f_0+\Delta f)\Delta d \sin\theta/c - (N-1)2\pi\Delta fr/c]} \end{bmatrix}, \qquad (57b)$$

$$\mathbf{u}(r, \theta)|_{\omega_{P-1}} =$$

$$\begin{bmatrix} 1, e^{-j[2\pi[f_0+\Delta f+(P-1)\Delta f_t]\Delta d \sin\theta/c - 2\pi\Delta fr/c - (P-1)2\pi\Delta f_t r/c]}, \\ \dots, e^{-j[(N-1)2\pi[f_0+\Delta f+(P-1)\Delta f_t]\Delta d \sin\theta/c - (N-1)2\pi\Delta fr/c - (P-1)2\pi\Delta f_t r/c]} \end{bmatrix}.$$

$$\text{(57c)}$$

The mean $\boldsymbol{\mu}$ and variance $\boldsymbol{\Gamma}$ of the data model x_u can be expressed as

$$\boldsymbol{\mu} = \mathbf{u}(r, \theta)\sqrt{\text{SNR}}, \tag{58}$$

$$\boldsymbol{\Gamma} = \mathbf{I}. \tag{59}$$

Thus, the Fisher information matrix (FIM) can be obtained as

$$\mathbf{F} = 2\text{Re}\left[\frac{d\mu^*}{d\beta}\Gamma^{-1}\frac{d\mu}{d\beta^T}\right], \tag{60}$$

where $\text{Re}[\cdot]$ stands for real value operation, $\beta = [r, \theta]^T$. Thus, the FIM of stepped frequency pulses FDA scheme can be written as

$$\mathbf{F}_S = 2 \cdot SNR$$

$$\cdot \begin{bmatrix} \sum_{p=0}^{P-1}\sum_{n=0}^{N-1}[\vartheta_p^2(n)] & \sum_{p=0}^{P-1}\sum_{n=0}^{N-1}[\vartheta_p(n) \cdot \rho_p(n)] \\ \sum_{p=0}^{P-1}\sum_{n=0}^{N-1}[\vartheta_p(n) \cdot \rho_p(n)] & \sum_{p=0}^{P-1}\sum_{n=0}^{N-1}[\rho_p^2(n)] \end{bmatrix}, \tag{61}$$

where

$$\vartheta_p(n) = n\frac{2\pi[f_0 + \Delta f + p\Delta f_t]\Delta d \cos\theta}{c}, \tag{62a}$$

$$\rho_p(n) = -n\frac{2\pi\Delta fr}{c} - p\frac{2\pi\Delta f_t r}{c}. \tag{62b}$$

Then the inverse matrix of the FIM can be expressed as

$$\mathbf{F}_S^{-1} = \frac{1}{F_{1,1}F_{2,2} - F_{1,2}F_{2,1}}\begin{bmatrix} F_{2,2} & -F_{2,1} \\ -F_{1,2} & F_{1,1} \end{bmatrix}. \tag{63}$$

Thus, the CRLB of the angle dimension and the range dimension can be solved, which are expressed as

$$\text{CRLB}_\theta = [\mathbf{F}_S^{-1}]_{1,1} = \frac{F_{2,2}}{F_{1,1}F_{2,2} - F_{1,2}F_{2,1}}, \tag{64a}$$

$$\text{CRLB}_r = [\mathbf{F}_S^{-1}]_{2,2} = \frac{F_{1,1}}{F_{1,1}F_{2,2} - F_{1,2}F_{2,1}}, \tag{64b}$$

where $[\cdot]_{i,j}$ represents the element in the ith row and jth column of the matrix.

Simulation results

In this section, the performance of proposed target localization scheme is verified by numerical simulation. Both single-target and dual-target situations are considered, and a comparison with the traditional double pulse FDA localization effects is provided.

Simulation parameters are considered as follows: the number of radar elements is $N = 16$, the reference frequency of the FDA transmit signal is $f_0 = 6$ GHz, the frequency offset increment between elements is $\Delta f = 2$ kHz, and the frequency increment between pulses is $\Delta f_t = 2$ kHz. In the simulation, Gaussian white noise with the same variance and zero mean is used.

Detecting a single target is considered first. Assuming that the target's position information is $(r_1, \theta_1) = (80\,\text{km}, 0°)$ under the condition of a signal-to-noise ratio (SNR) of -10 dB. The equivalent transmit beampattern of the traditional double-pulse FDA (DP-FDA) is shown in Fig. 4. It can be seen that the first step of DP-FDA is to use the phased array with $\Delta f = 0$ to estimate the angle parameters of the target. Since the transmit beampattern during $\Delta f \neq 0$ is coupled with range and angle parameters, the angle parameter from the first step is used as the prior information to estimate the range parameters of the target.

Figure 5 shows the equivalent transmit beampattern of CPD-based double-pulse FDA (CPD-DP-FDA) and CPD-based stepped frequency pulses FDA (CPD-SP-FDA). CPD-DP-FDA can decouple the range and angle of the equivalent transmit beampattern according to the data received by the radar. Thus, the maximum peak position of the beam can be used to locate the target. Since the radar's multi-carrier frequency time-division transmission provides a higher degree of freedom, the CPD-SP-FDA can form an equivalent beampattern of decoupling range and angle. Thus, the range parameter and angle parameter of the target can be estimated directly according to the maximum peak position of the beam.

Figure 6 shows the range and angle dimension beampatterns for parameter estimation with the three schemes. It can be observed that in the range dimension, the mainlobe of the CPD-SP-FDA is narrower and the sidelobes are lower, which is more conducive to the estimation of range parameters. In the angle dimension, the tensor decomposition effectively extracts the target angle information in the double pulse data, which achieve the selectivity in the angle dimension. Thus, the mainlobe of range-angle decoupling is formed in the beampattern, which shows that CPD-DP-FDA has certain advantages in angle parameter estimation. By deriving CRLB, it can be found that the number of pulses P, the number of array elements N, the frequency offset increment between array elements Δf, and the frequency increment between pulses Δf_t will all affect the estimation accuracy of the range parameter.

Next, parameter estimation for multiple targets is considered. Assuming that the coordinates of the two targets are $(r_1, \theta_1) = (70\,\text{km}, 20°)$ and $(r_2, \theta_2) = (80\,\text{km}, 0°)$ respectively. Figures 7 and 8 show the equivalent transmit beampatterns of the three schemes when two targets are considered. Since the two targets have different angle parameters, two angle parameters will be obtained in the first step of the traditional double pulse processing, as shown in Fig. 7(a). In the second step of estimating the range parameter, it cannot be used as *a priori* information to estimate the range parameter directly because the angle dimension peak information is not unique, as shown in Fig. 7(b). In Fig. 8(a), since the factor matrix containing the target information
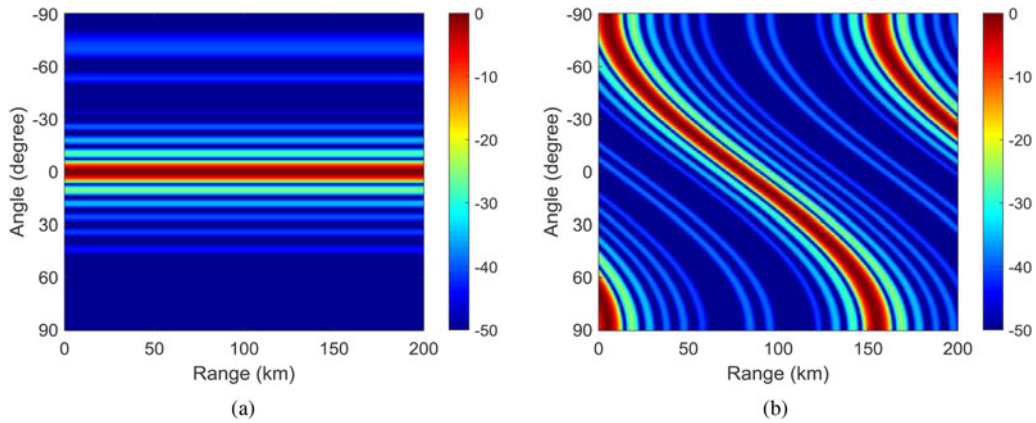
Fig. 4. Traditional double-pulse FDA equivalent transmit beampattern. (a) The first step. (b) The second step.
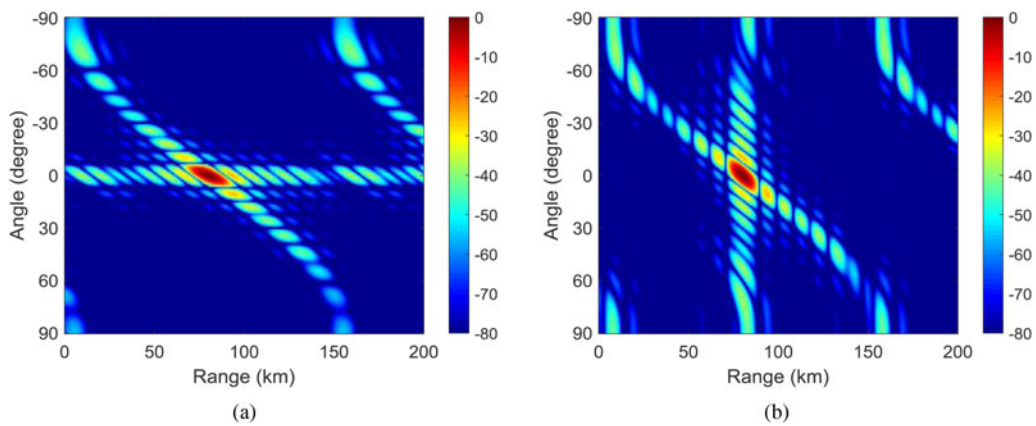

Fig. 5. FDA equivalent transmit beampattern based on CPD. (a) CPD-DP-FDA. (b) CPD-SP-FDA.
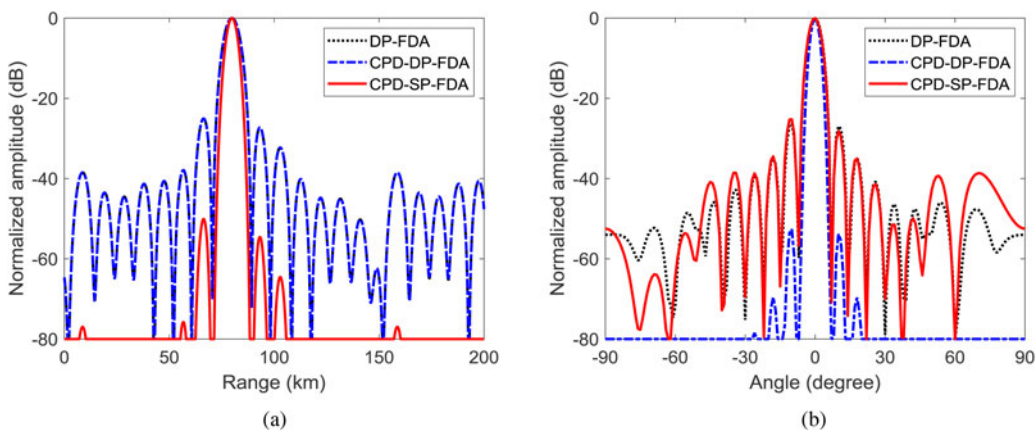

Fig. 6. Comparison of beam performance. (a) Range dimension. (b) Angle dimension.

after CPD is corresponding, CPD-DP-FDA realizes the automatic matching of the two target parameter estimates. Thus, there is no problem of ambiguity in parameter estimates. CPD-SP-FDA can also correspond to the positions of the two targets to the peak
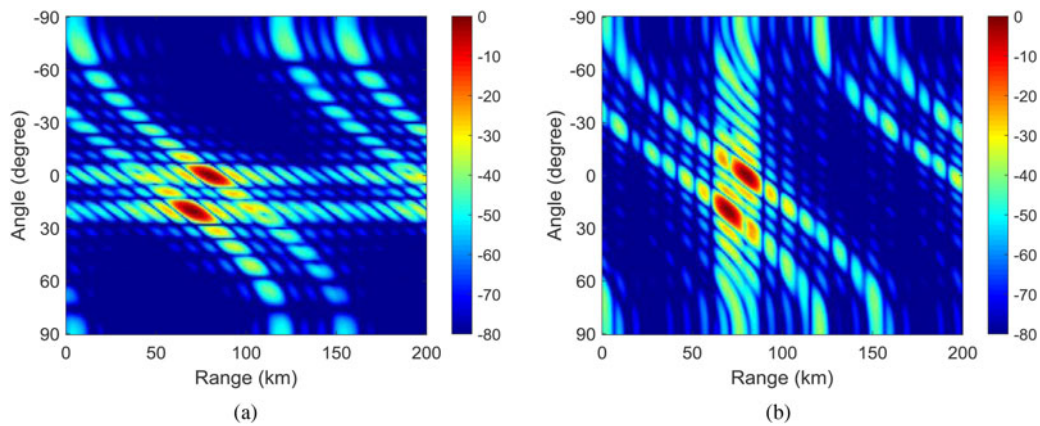
points, as shown in Fig. 8(b), which is conducive to parameter estimation of multiple targets.

DP-FDA will obtain two angle parameters $\hat{\theta}_1 = 0°$ and $\hat{\theta}_2 = 20°$ in the first step, and obtain four target points
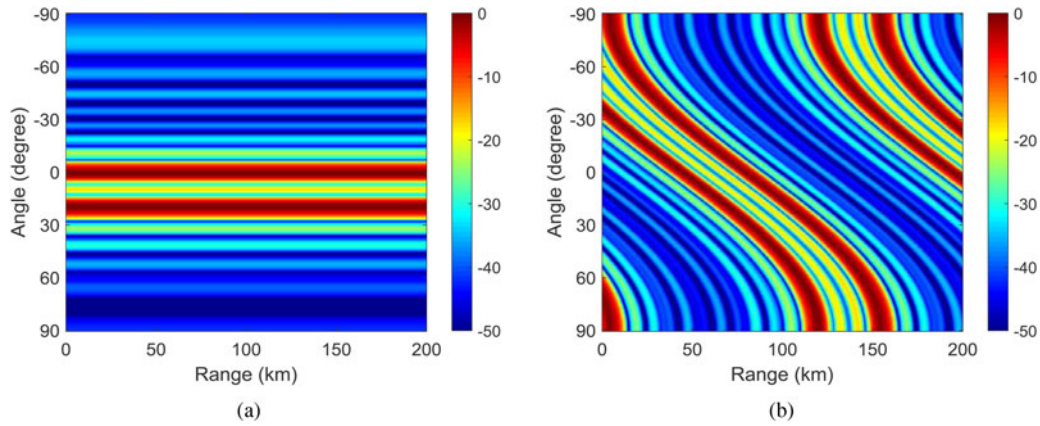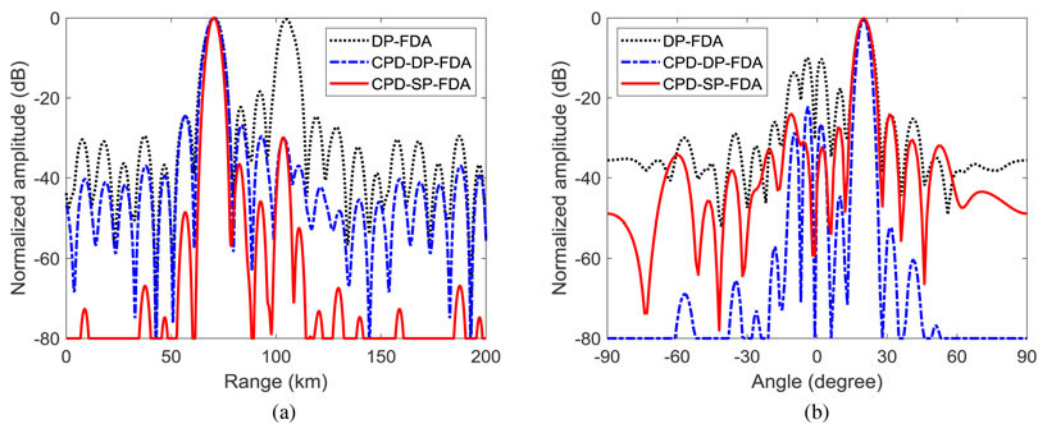
Fig. 7. Traditional double-pulse FDA equivalent transmit beampattern. (a) The first step. (b) The second step.

Fig. 8. FDA equivalent transmit beampattern based on CPD. (a) CPD-DP-FDA. (b) CPD-SP-FDA.

Fig. 9. Performance comparison of the first target beampattern. (a) Range dimension ($\theta = 20°$). (b) Angle dimension ($r = 70$ km).

(45 km, 0°), (70 km, 20°), (80 km, 0°), (105 km, 20°) in the subsequent parameter estimation in the second step. Thus, neither the number of real targets nor the position information under this scheme can be effectively distinguished. When CPD-DP-FDA scheme is used, automatic matching of target parameters is achieved during the solution process so that the parameters of

the two targets can be estimated. CPD-SP-FDA realizes the decoupling of the beampattern by time-division transmission. Thus, it can also estimate the parameters of the two targets. Figure 9 is a schematic diagram of the estimation effect of the first target. It can be found that the two CPD-based schemes have a unique mainlobe in both the range dimension and the
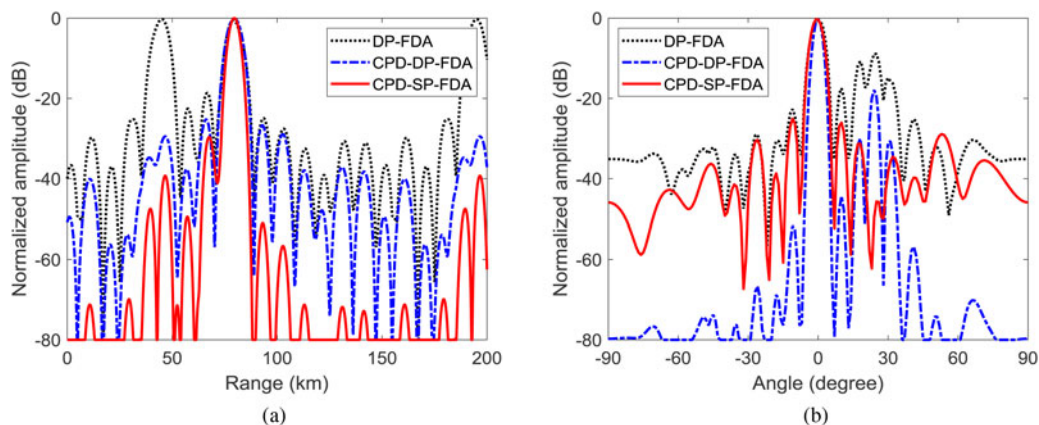
Fig. 10. Performance comparison of the second target beampattern. (a) Range dimension ($\theta = 0°$). (b) Angle dimension ($r = 80$ km).

Table 1. Comparison of different FDA methods

	Average BW_r (km)	Average BW_θ (°)	Unambiguity	Solution time (s)
DP-FDA	5	2.8	×	0.29
CPD-DP-FDA	5	2.8	√	2.71
CPD-SP-FDA	3.1	3.2	√	3.12

angle dimension, which can directly estimate the range and angle parameters of the first target.

Figure 10 shows a schematic diagram of the estimation effect of the second target. Similarly, the two CPD-based schemes have a unique mainlobe in the range dimension and the angle dimension, which have lower sidelobe levels. Thus, CPD-DP-FDA can effectively solve the problem of unclear target indication in DP-FDA. Then CPD-SP-FDA can also effectively estimate the range and angle parameters of multiple targets. Moreover, the half-power (−3 dB) contours of the equivalent target indication patterns corresponding to DP-FDA, CPD-DP-FDA, and CPD-SP-FDA are compared in Fig. 11. It is clearly shown that the scheme based on tensor decomposition can effectively solve the problem of uncertain multi-target parameter estimation, and the improvement of target parameter estimation performance brought by the stepped frequency pulse is also indicated. Table 1 shows the performance of beampattern in range and angle dimensions with different FDA methods. It can be seen from Table 1 that CPD-DP-FDA has the same BW with DP-FDA due to the same parameter while it can accomplish the discrimination of multiple targets. The BW_r of CPD-SP-FDA is 3.1 km, which is much better than that of other methods. In addition, due to the complex solution of factor matrices, the solution time of the CPD-based methods also grow.

Finally, Fig. 12 shows the CRLB performance comparison between the range dimension and the angle dimension. Because the traditional DP-FDA has ambiguity in multi-target parameter estimation, the two CPD-based schemes are compared in the figure. It can be seen that the parameter estimation effect of CPD-SP-FDA in the range dimension and the angle dimension is better than that of CPD-DP-FDA. Considering that SP-FDA uses two pulses, the performance of CRLB is still better than DP-FDA due to the higher degree of freedom provided by multiple carrier frequencies. As the number of pulses increases to 8,
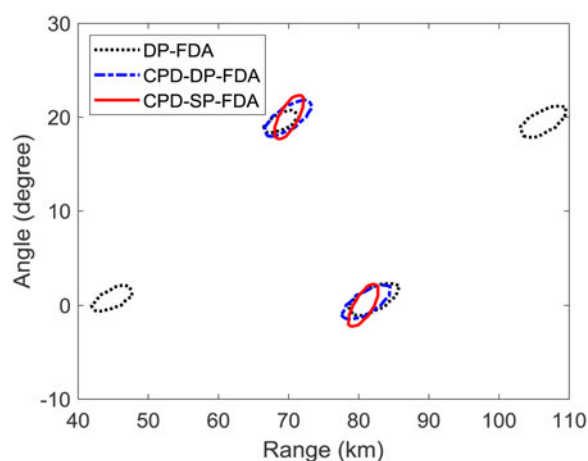

Fig. 11. Comparison of the −3 dB profile indicated by the equivalent beampattern.

the selectivity of SP-FDA in the range dimension is further improved, and CRLB performance is further optimized. However, it should be noted that the increase in the number of pulses increases the computational complexity of tensor decomposition, which means that the number of pulses needs to be reasonably selected according to the calculation ability in the actual application of the solution.

Although the proposed method is superior to other methods, the paper only considers scenarios with static targets. It means that extending the model to moving target scenarios requires the incorporation of new techniques. The introduction of cognitive radar ideas into FDA radar has recently attracted scholarly attention [33–36]. The cognitive-based processing model enables the detection and tracking of dynamic targets. Thus, it provides a reference for extending the model to dynamic target scenarios,
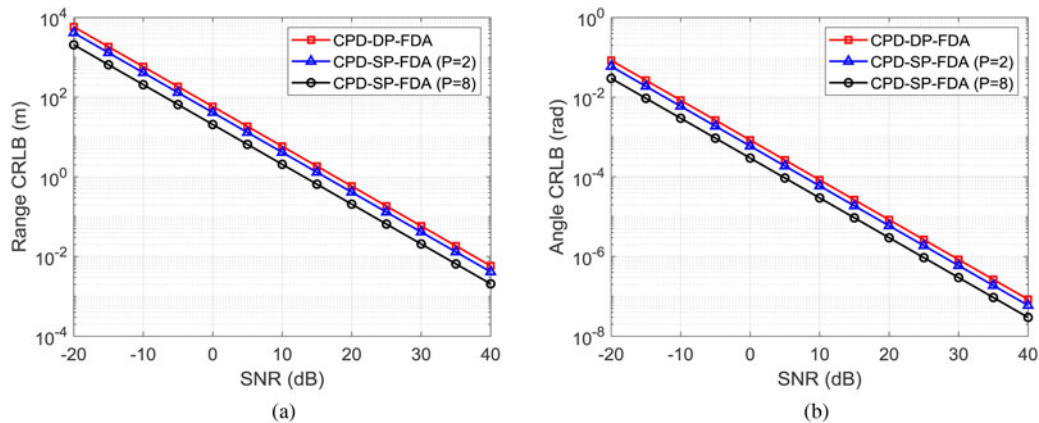
Fig. 12. Performance comparison of CRLB. (a) Range dimension. (b) Angle dimension.

which is the next research focus of system applicability enhancement.

Conclusion

In this paper, two new methods combined with tensor decomposition are presented for the two-dimensional parameter estimation of FDA-MIMO radar. The methods transform the traditional expression form of received data into the expression form of three-order tensor canonical polyadic decomposition, then the signal model of CPD-DP-FDA is established. With the help of the corresponding relationship of the factor matrix in the parallel factorization, the problem of ambiguity in the target indication of double pulse FDA is solved. To make full use of the advantages of multi-dimensional signal processing of tensor decomposition, a CPD-SP-FDA signal model based on stepped frequency pulses is established. In this way, the decoupling of the range and angle of the equivalent transmitting beam is realized, and the effectiveness of the proposed method is verified by numerical simulation. Compared with the performance of the traditional DP-FDA, the results show that the newly proposed scheme has better performance in terms of target indication and parameter estimation accuracy.

Moreover, the use of stepped frequency pulses for target localization results in high computational complexity. Thus, reasonable selection of the number of pulses and research on more efficient target parameter estimation methods become important factors that need to be considered in the future. In future work, applying the advantages of tensor signal processing to other radar research directions also should be considered.

References

1. **Antonik P, Wicks MC, Griffiths HD and Baker CJ** (2006) Frequency diverse array radars. *Proceedings of IEEE Radar Conference, Verona, Italy*, pp. 215–217.
2. **Sammartino PF, Baker CJ and Griffiths HD** (2013) Frequency diverse MIMO techniques for radar. *IEEE Transactions on Aerospace and Electronic Systems* **49**, 201–222.
3. **Wang WQ** (2013) Phased-MIMO radar with frequency diversity for range-dependent beamforming. *IEEE Sensors Journal* **13**, 1320–1328.
4. **Xu J, Liao G, Zhang Y, Ji H and Huang L** (2017) An adaptive range-angle-Doppler processing approach for FDA-MIMO radar using three-dimensional localization. *IEEE Journal of Selected Topics in Signal Processing* **11**, 309–320.
5. **Xiong J, Wang W and Gao K** (2018) FDA-MIMO radar range–angle estimation: CRLB, MSE, and resolution analysis. *IEEE Transactions on Aerospace and Electronic Systems* **54**, 284–294.
6. **Xu J, Liao G, Zhu S, Huang L and So HC** (2015) Joint range and angle estimation using MIMO radar with frequency diverse array. *IEEE Transactions on Signal Processing* **63**, 3396–3410.
7. **Xu J, Liao G, Zhu S and So HC** (2015) Deceptive jamming suppression with frequency diverse MIMO radar. *Signal Processing* **113**, 9–17.
8. **Gao K, Shao H, Chen H, Cai J and Wang WQ** (2015) Impact of frequency increment errors on frequency diverse array MIMO in adaptive beamforming and target localization. *Digital Signal Processing* **44**, 58–67.
9. **Gao K, Wang WQ and Cai J** (2016) Frequency diverse array and MIMO hybrid radar transmitter design via Cramer-Rao lower bound minimization. *IET Radar, Sonar & Navigation* **10**, 1660–1670.
10. **Zhu Y, Liu L, Lu Z and Zhang S** (2019) Target detection performance analysis of FDA-MIMO radar. *IEEE Access* **7**, 164276–164285.
11. **Wang WQ** (2013) Range-angle dependent transmit beampattern synthesis for linear frequency diverse arrays. *IEEE Transactions on Antennas and Propagation* **61**, 4073–4081.
12. **Wang WQ and Shao HZ** (2014) Range-angle localization of targets by a double-pulse frequency diverse array radar. *IEEE Journal on Selected Topics in Signal Processing* **8**, 106–144.
13. **Khan W, Qureshi IM, Basit A and Zubair M** (2015) A double pulse MIMO frequency diverse array radar for improved range-angle localization of target. *Wireless Personal Communications* **82**, 2199–2213.
14. **Lan L, Xu J, Liao G, Zhang Y and Huang Y** (2019) Precise response control of transmit-receive two-dimensional beampattern in FDA-MIMO radar. *Proceedings of 2019 27th European Signal Processing Conference (EUSIPCO), A Coruna, Spain*, pp. 1–5.
15. **Lan L, Marino A, Aubry A, De Maio A, Liao G and Xu J** (2020) Design of adaptive detectors for FDA-MIMO radar. *Proceedings of 2020 IEEE 11th Sensor Array and Multichannel Signal Processing Workshop (SAM), Hangzhou, China*, pp. 1–5.
16. **Wang Y, Huang G and Li W** (2017) Transmit beampattern design in range and angle domains for MIMO frequency diverse array radar. *IEEE Antennas and Propagation Letters* **16**, 1–4.
17. **Gao K, Shao H, Cai J, Chen H and Wang WQ** (2015) Frequency diverse array MIMO radar adaptive beamforming with range-dependent interference suppression in target localization. *International Journal of Antennas and Propagation* **1**, 1–10.

18. **Wang W, So HC and Farina A** (2019) FDA-MIMO signal processing for mainlobe jammer suppression. *Proceedings 2019 27th European Signal Processing Conference (EUSIPCO), A Coruna, Spain*, pp. 1–5.

19. **Wang H, Liao G, Xu J and Zhu S** (2020) Space-time matched filter design for interference suppression in coherent frequency diverse array. *IET Signal Processing* **14**, 175–181.

20. **Wang Y and Zhu S** (2020) Main-beam range deceptive jamming suppression with simulated annealing FDA-MIMO radar. *IEEE Sensors Journal* **20**, 9056–9070.

21. **Zhang X, Cao D and Xu L** (2019) Joint polarisation and frequency diversity for deceptive jamming suppression in MIMO radar. *IET Radar, Sonar & Navigation* **13**, 263–271.

22. **Yao AM, Wu W and Fang DG** (2017) Solutions of time-invariant spatial focusing for multi-targets using time modulated frequency diverse antenna arrays. *IEEE Transactions on Antennas and Propagation* **65**, 552–566.

23. **Yao AM, Rocca P, Wu W, Massa A and Fang DG** (2017) Synthesis of time-modulated frequency diverse arrays for short-range multi-focusing. *IEEE Journal of Selected Topics in Signal Processing* **11**, 282–294.

24. **Tan M, Wang C and Li Z** (2020) Correction analysis of frequency diverse array radar about time. *IEEE Transactions on Antennas and Propagation* **69**, 834–847.

25. **Bro R** (1997) PARAFAC. Tutorial and applications. *Chemometrics and Intelligent Laboratory Systems* **38**, 149–171.

26. **De Lathauwer L, De Moor B and Vandewalle J** (2000) A multilinear singular value de-composition. *SIAM Journal on Matrix Analysis and Applications* **21**, 1253–1278.

27. **Sidiropoulos ND, Bro R and Giannakis GB** (2000) Parallel factor analysis in sensor array processing. *IEEE Transactions on Signal Processing* **48**, 2377–2388.

28. **Nion D and Sidiropoulos ND** (2010) Tensor algebra and multidimensional harmonic retrieval in signal processing for MIMO radar. *IEEE Transactions on Signal Processing* **58**, 5693–5705.

29. **Zhang X, Xu Z, Xu L and Xu D** (2011) Trilinear decomposition-based transmit angle and receive angle estimation for multiple-input multiple-output radar. *IET Radar, Sonar & Navigation* **5**, 626–631.

30. **Wen F, Zhang Z and Zhang G** (2019) Joint DOD and DOA estimation for bistatic MIMO radar: a covariance trilinear decomposition perspective. *IEEE Access* **7**, 53273–53283.

31. **Xu T, Yang Y, Huang M, Wang H, Wu D and Yi Q** (2020) Tensor-based angle and range estimation method in monostatic FDA-MIMO radar. *Mathematical Problems in Engineering*, **2020**.

32. **Cheng L, Wu Y-C and Poor HV** (2016) Probabilistic tensor canonical polyadic decomposition with orthogonal factors. *IEEE Transactions on Signal Processing* **65**, 663–676.

33. **Wang WQ** (2016) Cognitive frequency diverse array radar with situational awareness. *IET Radar Sonar & Navigation* **10**, 359–369.

34. **Wang WQ** (2016) Moving-target tracking by cognitive RF stealth radar using frequency diverse array antenna. *IEEE Transactions on Geoscience and Remote Sensing* **54**, 3764–3773.

35. **Gui R, Wang WQ, Pan Y and Xu J** (2018) Cognitive target tracking via angle-range-Doppler estimation with transmit subaperturing FDA radar. *IEEE Journal of Selected Topics in Signal Processing* **12**, 76–89.

36. **Basit A, Wang WQ, Nusenu SY and Zheng Z** (2019) Cognitive FDA-MIMO With channel uncertainty information for target tracking. *IEEE Transactions on Cognitive Communications and Networking* **5**, 963–975.
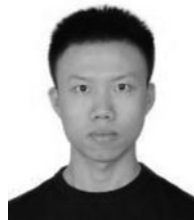
Yibin Liu received his B.E. degree in electronic engineering from Air Force Engineering University, Xi'an, China, in 2020. Now he is a postgraduate student in Air Force Engineering University. His current research interests include radar signal processing and robust adaptive beamforming.

Chunyang Wang received the Master's degree and Doctor's degree in Electromagnetic Field and Microwave Technique from Air Force Engineering University, Xi'an, China, in 1991 and 2004, respectively. He is currently a professor in the Air and Missile Defense College, Air Force Engineering University, Xi'an, China. His current research interests include radar signal processing, radar jamming, and anti-jamming technologies.
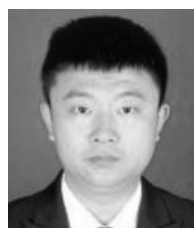
Jian Gong received his M.S. degree in circuits and systems from Air Force Engineering University, Xi'an, China, in 2009. He received his Ph.D. in pattern recognition and intelligent systems from Xidian University, Xi'an, China, in 2018. His research interests include signal detection and parameter estimation in array signal processing.

Ming Tan received the M.S. and Ph.D. degrees from Air Force Engineering University, Xi'an, China, in 2016 and 2020, respectively. He is currently a lecturer at the National University of Defense Technology (NUDT). His research interests include array signal processing, waveform diverse array, and electronic countermeasure.